EXTENDED PDF FORMAT
SPONSORED BY
usb
Products from Affymetrix
www.usbweb.com

Unsupervised Natural Experience Rapidly Alters Invariant Object Representation in Visual Cortex

Nuo Li, *et al.*

Science **321**, 1502 (2008);
DOI: 10.1126/science.1160028

The following resources related to this article are available online at www.sciencemag.org (this information is current as of October 16, 2008):

Updated information and services, including high-resolution figures, can be found in the online version of this article at:
http://www.sciencemag.org/cgi/content/full/321/5895/1502

Supporting Online Material can be found at:
http://www.sciencemag.org/cgi/content/full/321/5895/1502/DC1

This article **cites 45 articles**, 15 of which can be accessed for free:
http://www.sciencemag.org/cgi/content/full/321/5895/1502#otherarticles

This article has been **cited by** 1 articles hosted by HighWire Press; see:
http://www.sciencemag.org/cgi/content/full/321/5895/1502#otherarticles

This article appears in the following **subject collections**:
Neuroscience
http://www.sciencemag.org/cgi/collection/neuroscience

Information about obtaining **reprints** of this article or about obtaining **permission to reproduce this article** in whole or in part can be found at:
http://www.sciencemag.org/about/permissions.dtl

Downloaded from www.sciencemag.org on October 16, 2008

Science (print ISSN 0036-8075; online ISSN 1095-9203) is published weekly, except the last week in December, by the American Association for the Advancement of Science, 1200 New York Avenue NW, Washington, DC 20005. Copyright 2008 by the American Association for the Advancement of Science; all rights reserved. The title *Science* is a registered trademark of AAAS.

WT cells. Finally, we cotransfected SUM149PT cells with constructs encoding both FBXW7 and HA-ubiquitin, and found that ubiquitination of mTOR was restored by exogenous *FBXW7* expression (Fig. 2E). Thus, ubiquitination of mTOR is largely, if not exclusively, mediated by binding to FBXW7.

As *FBXW7* and *PTEN* both affect signaling through mTOR, we examined the genetic status of both genes in a panel of 53 breast cancer cell lines (*11*). Quantitative TaqMan real-time polymerase chain reaction (PCR) assays of the number of copies of *FBXW7* and *PTEN* genes in each of the cell lines were in good concordance with data found by bacterial artificial chromosome (BAC) comparative genomic hybridization (CGH) microarray (see table S1). Most of the breast cancer cell lines that exhibited loss of a single copy of *FBXW7* (23 out of 53, Fig. 3A) did not show corresponding loss of *PTEN*. In contrast, of the 14 lines that showed loss of a single copy of *PTEN* (Fig. 3A), only one had also lost a copy of *FBXW7*, which suggested that *FBXW7* and *PTEN* show some functional redundancy in tumor development. Similar results were obtained by examination of the copy number status of genomic regions containing *FBXW7* and *PTEN* genes in three independent human primary breast cancer sets for which BAC CGH microarray data were available (*12*–*14*). From a total of 450 tumor and cell line DNA samples shown in Fig. 3, A to D, only 4 had lost a copies of the regions containing both genes, a result that is unlikely to be a consequence of random genetic alterations ($P = 4.9 \times 10^{-7}$).

We also considered the possibility that other somatic changes such as point mutations or gene-silencing events could affect the results. The *FBXW7* gene continued to be expressed in all 25 breast cancer cell lines examined (fig. S8), which indicated that no gene silencing had occurred, although very low levels were found in five cell lines [lanes 10, 13, 14, 16, and 20 (fig. S8)]. All of these lines had lost one copy of the *FBXW7* gene except one (SUM149PT, lane 16), in which a point mutation was detected (table S1). The *PTEN* gene was found to be silent in two cell lines (fig. S8, lanes 11 and 12), and both had lost one copy of the *PTEN* gene. Three mutations in *PTEN* were found (fig. S8 and table S1). Thus, gene silencing (for example, by promoter methylation) or point mutations in *FBXW7* and *PTEN* are relatively rare mechanisms of inactivation of these genes, in comparison with single-copy deletions. These data are further compatible with the identification of both genes as haplo-insufficient tumor suppressors (*3*, *15*, *16*).

Because deletion or mutation of *FBXW7* in human breast cancer cells leads to increased levels of mTOR, we tested the possibility that cells harboring these deletions may show increased sensitivity to the mTOR inhibitor rapamycin. We treated two breast cancer cell lines, SUM149PT cells (homozygous *FBXW7* mutations) and MDA-MB453 cells (wild-type *FBXW7*) with rapamycin and counted numbers of viable cells. SUM149PT cells proved to be very sensitive to this treatment [median inhibitory concentration (IC_{50}) < 200 nM], whereas MDA-MB453 cells were relatively resistant (IC_{50} > 2 μM) (Fig. 4A). In nude mouse xenografts, groups of five mice were injected with both cell lines, one on each flank, and were treated by intraperitoneal injection with rapamycin over an 11-day period. The SUM149PT cells showed a relative decrease in size followed by stable tumor growth, whereas the MDA-MB453 cells were relatively unaffected by treatment (Fig. 4B).

An additional set of 10 breast cancer cell lines was treated with rapamycin at concentrations of 200 and 400 nM. Cells with deletion or mutation of *FBXW7* (HBL100, 600MPE, SUM149PT, HCC3153, and HCC1143) or *PTEN* (HCC1937 and HCC3153) showed significant sensitivity to killing by rapamycin, although the magnitude of the effect varied (*17*) (Fig. 4C). To establish a direct link between loss of FBXW7 and rapamycin sensitivity, we down-regulated expression levels of FBXW7 using short hairpin RNA (shRNA) (*18*) in the rapamycin-resistant MDA-MB453 cells, which resulted in an increase in sensitivity to this drug [IC_{50}< 0.8 μM (Fig. 4D)].

Our findings implicate FBXW7 in an evolutionarily conserved pathway that controls regulation of mTOR protein levels. Because FBXW7 is a haploinsufficient tumor suppressor that undergoes heterozygous loss in a substantial proportion of human tumors, the data suggest new approaches to reduce mTOR levels in cancers by the use of drugs that may reactivate the remaining copy of FBXW7 in a similar way that nutlins (small-molecule MDM2-antagonists) have been shown to activate wild-type copies of p53 in human tumors (*19*). Loss of FBXW7 may also be a useful biomarker for sensitivity of human tumors to inhibitors of the mTOR pathway.

References and Notes

1. M. Welcker, B. E. Clurman, *Nat. Rev. Cancer* **8**, 83 (2008).
2. S. Akhoondi *et al.*, *Cancer Res.* **67**, 9006 (2007).
3. J. H. Mao *et al.*, *Nature* **432**, 775 (2004).
4. H. Rajagopalan *et al.*, *Nature* **428**, 77 (2004).
5. M. Yada *et al.*, *EMBO J.* **23**, 2116 (2004).
6. M. Welcker *et al.*, *Proc. Natl. Acad. Sci. U.S.A.* **101**, 9085 (2004).
7. Z. Kemp *et al.*, *Cancer Res.* **65**, 11361 (2005).
8. Single-letter abbreviations for the amino acid residues are as follows: A, Ala; C, Cys; D, Asp; E, Glu; F, Phe; G, Gly; H, His; I, Ile; K, Lys; L, Leu; M, Met; N, Asn; P, Pro; Q, Gln; R, Arg; S, Ser; T, Thr; V, Val; W, Trp; Y, Tyr; and X, any amino acid.
9. G. Wu *et al.*, *Mol. Cell. Biol.* **21**, 7403 (2001).
10. H. Strohmaier *et al.*, *Nature* **413**, 316 (2001).
11. R. M. Neve *et al.*, *Cancer Cell* **10**, 515 (2006).
12. J. Climent *et al.*, *Cancer Res.* **67**, 818 (2007).
13. K. Chin *et al.*, *Cancer Cell* **10**, 529 (2006).
14. J. Fridlyand *et al.*, *BMC Cancer* **6**, 96 (2006).
15. J. H. Mao *et al.*, *Oncogene* **22**, 8379 (2003).
16. A. Di Cristofano, B. Pesce, C. Cordon-Cardo, P. P. Pandolfi, *Nat. Genet.* **19**, 348 (1998).
17. L. S. Steelman *et al.*, *Oncogene* **27**, 4086 (2008).
18. M. Welcker, A. Orian, J. E. Grim, R. N. Eisenman, B. E. Clurman, *Curr. Biol.* **14**, 1852 (2004).
19. J. K. Buolamwini *et al.*, *Curr. Cancer Drug Targets* **5**, 57 (2005).

20. We thank B. Vogelstein for providing us with the HCT116 WT, HCT116 *FBXW7*$^{-/-}$, DLD1 wild-type, and DLD1 *FBXW7*$^{-/-}$ cell lines; K.I. Nakayama for providing *Fbxw7* knockout mice and vectors (HA-FBXW7 and HA-FBXW7ΔF); and O. Tetsu for vector encoding HA-ubiquitin. These studies were supported by NCI grant U01 CA84244 and the U.S. Department of Energy (DE-FG02-03ER63630) to A.B., the University of California at San Francisco Research-Evaluation Allocation Committee (REAC) to J.-H.M. A.B. acknowledges support from the Barbara Bass Bakar Chair of Cancer Genetics.

Supporting Online Material

www.sciencemag.org/cgi/content/full/321/5895/1499/DC1
Materials and Methods
Figs. S1 to S8
Table S1

9 July 2008; accepted 11 August 2008
10.1126/science.1162981

Unsupervised Natural Experience Rapidly Alters Invariant Object Representation in Visual Cortex

Nuo Li and James J. DiCarlo*

Object recognition is challenging because each object produces myriad retinal images. Responses of neurons from the inferior temporal cortex (IT) are selective to different objects, yet tolerant ("invariant") to changes in object position, scale, and pose. How does the brain construct this neuronal tolerance? We report a form of neuronal learning that suggests the underlying solution. Targeted alteration of the natural temporal contiguity of visual experience caused specific changes in IT position tolerance. This unsupervised temporal slowness learning (UTL) was substantial, increased with experience, and was significant in single IT neurons after just 1 hour. Together with previous theoretical work and human object perception experiments, we speculate that UTL may reflect the mechanism by which the visual stream builds and maintains tolerant object representations.

When presented with a visual image, primates can rapidly (<200 ms) recognize objects despite large variations in object position, scale, and pose (*1*, *2*). This ability likely derives from the responses of neurons at high levels of the primate ventral visual stream (*3*–*5*). But how are these powerful "invariant" neuronal object representations built

Downloaded from www.sciencemag.org on October 16, 2008

by the visual system? On the basis of theoretical (*6*–*11*) and behavioral (*12*, *13*) work, one possibility is that tolerance ("invariance") is learned from the temporal contiguity of object features during natural visual experience, potentially in an unsupervised manner. Specifically, during natural visual experience, objects tend to remain present for seconds or longer, while object motion or viewer motion (e.g., eye movements) tends to cause rapid changes in the retinal image cast by each object over shorter time intervals (hundreds of ms). The ventral visual stream could construct a tolerant object representation by taking advantage of this natural tendency for temporally contiguous retinal images to belong to the same object. If this hypothesis is correct, it might be possible to uncover a neuronal signature of the underlying learning by using targeted alteration of those spatiotemporal statistics (*12*, *13*).

To look for such a signature, we focused on position tolerance. If two objects consistently swapped identity across temporally contiguous changes in retinal position then, after sufficient experience in this "altered" visual world, the visual system might incorrectly associate the neural representations of those objects viewed at different positions into a single object representation (*12*, *13*). We focused on the top level of the primate ventral visual stream, the inferior temporal cortex (IT), where many individual neurons possess position tolerance—they respond preferentially to different objects, and that selectivity is largely maintained across changes in object retinal position, even when images are simply presented to a fixating animal (*14*, *15*).

We tested a strong, "online" form of the temporal contiguity hypothesis—two monkeys visually explored an altered visual world (Fig. 1A, "Exposure phase"), and we paused every ~15 min to test each IT neuron for any change in position tolerance produced by that altered experience (Fig. 1A, "Test phase"). We concentrated on each neuron's responses to two objects that elicited strong (object "P", preferred) and moderate (object "N", nonpreferred) responses, and we tested the position tolerance of that object selectivity by briefly presenting each object at 3° above, below, or at the center of gaze (*16*) (fig. S1). All neuronal data reported in this study were obtained in these test phases: animal tasks unrelated to the test stimuli; no attentional cueing; and completely randomized, brief presentations of test stimuli (*16*). We alternated between these two phases (test phase ~5 min; exposure phase ~15 min) until neuronal isolation was lost.

To create the altered visual world ("Exposure phase" in Fig. 1A), each monkey freely viewed the video monitor on which isolated objects appeared intermittently, and its only task was to freely look at each object. This exposure "task" is a natural, automatic primate behavior in that it requires no training. However, by means of real-time eye-tracking (*17*), the images that played out on the monkey's retina during exploration of this world were under precise experimental control (*16*). The objects were placed on the video monitor so as to (initially) cast their image at one of two possible retinal positions (+3° or −3°). One of these retinal positions was pre-chosen for targeted alteration in visual experience (the "swap" position; counterbalanced across neurons) (Fig. 1B) (*16*); the other position acted as a control (the "non-swap" position). The monkey quickly saccaded to each object (mean: 108 ms after object appearance), which rapidly brought the object image to the center of its retina (mean saccade duration 23 ms). When the object had appeared at the non-swap position, its identity remained stable as the monkey saccaded to it, typical of real-world visual experience ("Normal exposure", Fig. 1A) (*16*). However, when the object had appeared at the swap position, it was always replaced by the other object (e.g., P→N) as the monkey saccaded to it (Fig. 1A, "Swap exposure"). This experience manipulation took advantage of the fact that primates are effectively blind during the brief time it takes to complete a saccade (*18*). It consistently made the image of one object at a peripheral retinal position (swap position) temporally contiguous with the retinal image of the other object at the center of the retina (Fig. 1).

We recorded from 101 IT neurons while the monkeys were exposed to this altered visual world (isolation held for at least two test phases; $n = 50$ in monkey 1; 51 in monkey 2). For each neuron, we measured its object selectivity at each position as the difference in response to the two objects (P − N; all key effects were also found with a contrast index of selectivity) (fig. S6). We found that, at the swap position, IT neurons (on average) decreased their initial object selectivity

McGovern Institute for Brain Research and Department of Brain and Cognitive Sciences, Massachusetts Institute of Technology, Cambridge, MA 02139, USA.

*To whom correspondence should be addressed. E-mail: dicarlo@mit.edu

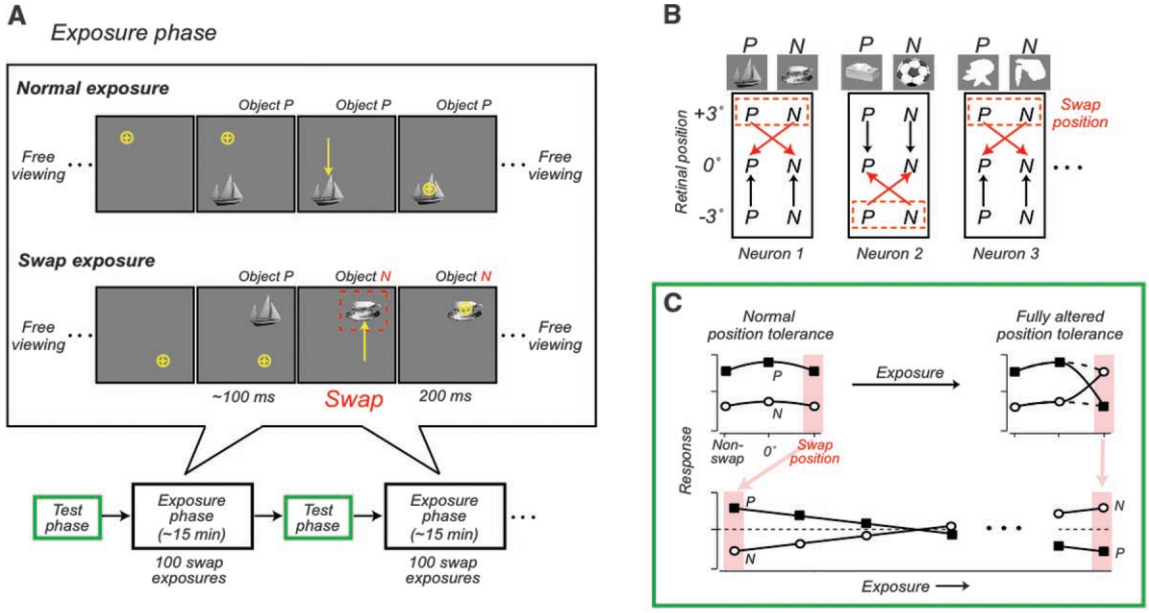

Fig. 1. Experimental design and predictions. (**A**) IT responses were tested in "Test phase" (green boxes, see text), which alternated with "Exposure phase." Each exposure phase consisted of 100 normal exposures (50 P→P, 50 N→N) and 100 swap exposures (50 P→N, 50 N→P). Stimulus size was 1.5° (*16*). (**B**) Each box shows the exposure-phase design for a single neuron. Arrows show the saccade-induced temporal contiguity of retinal images (arrowheads point to the retinal images occurring later in time, i.e., at the end of the saccade). The swap position was strictly alternated (neuron-by-neuron) so that it was counterbalanced across neurons. (**C**) Prediction for responses collected in the test phase: If the visual system builds tolerance using temporal contiguity (here driven by saccades), the swap exposure should cause incorrect grouping of two different object images (here P and N). Thus, the predicted effect is a decrease in object selectivity at the swap position that increases with increasing exposure (in the limit, reversing object preference), and little or no change in object selectivity at the non-swap position.

Downloaded from www.sciencemag.org on October 16, 2008

for P over N, and this change in object selectivity grew monotonically stronger with increasing numbers of swap exposure trials (Fig. 2, A and C). However, the same IT neurons showed (Fig. 2A) no average change in their object selectivity at the equally eccentric control position (non-swap position), and little change in their object selectivity among two other (nonexposed) control objects (see below).

Because each IT neuron was tested for different amounts of exposure time, we first computed a net object selectivity change, Δ(P − N), in the IT population by using the first and last available test phase data for each neuron. The prediction was that Δ(P − N) should be negative (i.e., in the direction of object preference reversal), and greatest at the swap position (Fig. 1C). This prediction was borne out (Fig. 3A). The position specificity of the experience-induced changes in object selectivity was confirmed by two different statistical approaches: (i) a direct comparison of Δ(P − N) between the swap and non-swap position (n = 101; P = 0.005, one-tailed paired t test); (ii) a significant interaction between position and exposure—that is, object selectivity decreased at the swap position with increasing amounts of exposure [P = 0.009 by one-tailed bootstrap; P = 0.007 by one-tailed permutation test; tests were done on (P − N)].

The changes in object selectivity at the swap position were also largely shape-specific. For 88 of the 101 neurons, we monitored the neuron's selectivity among two control objects not shown to the animals during the exposure phase (chosen similar to the way in which the P and N objects were selected, fully interleaved testing in each test phase) (*16*). Across the IT population, control object selectivity at the swap position did not significantly change (Fig. 2A), and the swap object selectivity changed significantly more than the control object selectivity (Fig. 3B) (n = 88, P = 0.009, one-tailed paired t test of swap versus control objects at the swap position).

These changes in object selectivity were substantial (average change of ~5 spikes/s per 400 exposures at the swap position) (Figs. 2C and 3C) and were readily apparent and highly significant at the population level. In the face of well-known Poisson spiking variability (*19*, *20*), these effects were only weakly visible in most single IT neurons recorded for short durations, but were much more apparent over the maximal 1-hour exposure time that we could hold neurons in isolation (Fig. 2C, lower panels). To determine if the object selectivity changes continued to grow even larger with longer periods of exposure, we next recorded multi-unit activity (MUA) in one animal (monkey 2), which allowed us to record from a number of (nonisolated) neurons around the electrode tip (which all tend to have similar selectivity) (*21*, *22*) while the monkey was exposed to the altered visual world for the entire experiment (~2 hours) (*16*). The MUA data replicated the single-unit results—a change in object selectivity only at the swap position (Fig. 2C) ("position × exposure" interaction: P = 0.03, one-tailed bootstrap; P = 0.014, one-tailed permutation test; n = 10). Furthermore, the MUA object selectivity change at the swap position continued to increase as the animal received even more exposure to the altered visual world, followed a very similar time course in the rate of object selectivity change (~5 spikes/s per 400 exposures) (Fig. 3C), and even showed a slight reversal in object selectivity (N > P in Fig. 4D).

Our main results were similar in magnitude (Fig. 3, A and B) and statistically significant in each of the two monkeys (monkey 1: P = 0.019; monkey 2: P = 0.0192; one-tailed t test). Each monkey performed a different task during the test phase (*16*), suggesting that these neuronal changes are not task dependent.

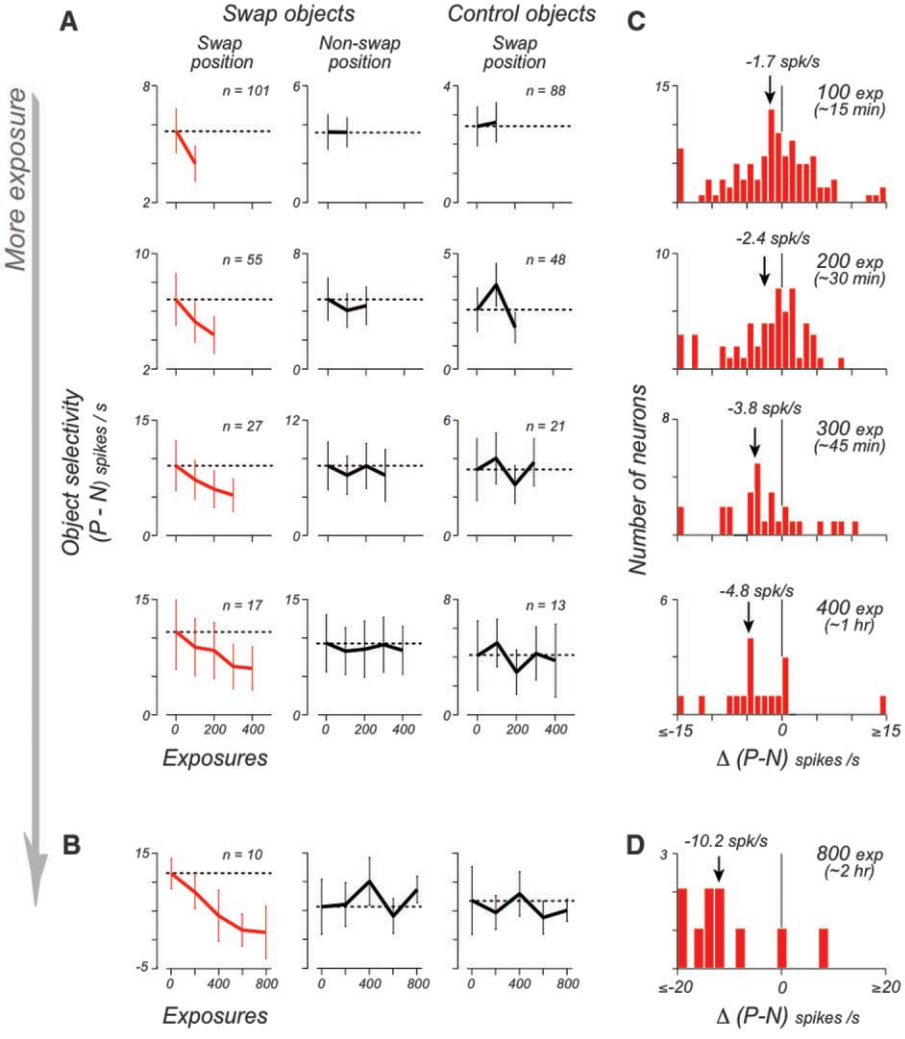

Fig. 2. Change in the population object selectivity. (**A**) Mean population object selectivity at the swap and (equally eccentric) non-swap position, and for control objects at the swap position. Each row of plots shows effect among all neurons held for at least the indicated amount of exposure (e.g., top row shows all neurons held for more than 100 swap exposures—including the neurons from the lower rows). The object selectivity for each neuron was the difference in its response to object P and N. To avoid any bias in this estimate, for each neuron we defined the labels "P" (preferred) and "N" by using a portion of the pre-exposure data (10 repetitions) to determine these labels, and the reminder to compute the displayed results in all analyses using these labels. Though there was, by chance, slightly greater initial selectivity at the swap position, this cannot explain the position specificity of the observed change in selectivity (table S2). (**B**) Mean population object selectivity of 10 multi-unit sites. Error bars (A and B) are SEMs. (**C**) Histograms of the object selectivity change at the swap position, $\Delta(P - N) = (P - N)_{\text{post-exposure}} - (P - N)_{\text{pre-exposure}}$. The arrows indicate the means of the distributions. The mean Δ(P − N) at the non-swap position was −0.01, −0.5, −0.9, and −0.9 spikes/s, respectively. The variability around that mean (i.e., distribution along the x axis) is commensurate with repeated measurements in the face of known Poisson spiking variability (fig. S11). (**D**) Object selectivity changes at the multi-unit sites. The mean Δ(P − N) at the non-swap position was 1.6 spikes/s.

Downloaded from www.sciencemag.org on October 16, 2008

Because we selected the objects P and N so that they both tended to drive the neuron (*16*), the population distribution of selectivity for P and N at each position was very broad [95% range: (−5.7 to 31.0 spikes/s) pooled across position; n = 101]. However, our main prediction assumes that the IT neurons were initially object-selective (i.e., the response to object P was greater than to object N). Consistent with this, neurons in our population with no initial object selectivity at the center of gaze showed little average change in object selectivity at the swap position with exposure (fig. S5). To test the learning effect in the most selective IT neurons, we selected the neurons with significant object selectivity [n = 52 of 101 neurons; two-way analysis of variance (2 objects × 3 positions), $P < 0.05$, significant main object effect or interaction]. Among this smaller number of object-selective neurons, the learning effect remained highly significant and still specific to the swap position ($P = 0.002$ by t test; $P = 0.009$ by bootstrap; $P = 0.004$ by permutation test).

To further characterize the response changes to individual objects, we closely examined the selective neurons held for at least 300 exposures (n = 28 of 52 neurons) and the multi-unit sites (n = 10). For each neuron and site, we used linear regression to measure any trend in response to each object as a function of exposure time (Fig. 4A). Changes in response to P and N at the swap position were apparent in a fraction of single neurons and sites (Fig. 4A), and statistically significant object selectivity change was encountered in 12 of 38 (32%) instances (Fig. 4C) (*16*). Across our neuronal population, the change in object selectivity at the swap position was due to both a decreased response to object P and an increased response to object N (approximately equal change) (Fig. 4B). These response changes were highly visible in the single-units and multi-units held for the longest exposure times (Fig. 4D).

These changes in the position profile of IT object selectivity (i.e., position tolerance) cannot be explained by changes in attention or by adaptation (fig. S10). First, a simple fatigue-adaptation model cannot explain the position specificity of the changes because, during the recording of each neuron, each object was experienced equally often at the swap and non-swap positions (also see additional control in table S2). Second, we measured these object selectivity changes with briefly presented, fully randomized stimuli while the monkeys performed tasks unrelated to the stimuli (*16*), which argues against an attentional account. Third, both of these explanations predict response decrease to all objects at the swap position, yet we found that the change in object selectivity at the swap position was due to an increase in response to object N (+2.3 spikes/s per 400 swap exposures) as well as a decrease in response to object P (−3.0 spikes/s per 400 swap exposures) (Fig. 4). Fourth, neither possibility can explain the shape specificity of the changes.

We term this effect "unsupervised temporal slowness learning" (UTL), because the selectivity changes depend on the temporal contiguity of object images on the retina and are consistent with the hypothesis that the natural stability (slowness) of object identity instructs the learning without external supervision (*6*–*11*). Our current data as well as previous human object perception experiments (*12*) cannot rule out the possibility that the brain's saccade-generation mechanisms or the associated attentional mechanisms (*23*, *24*) may also be needed. Indeed, eye-movement signals are present in the ventral stream (*25*, *26*). The relatively fast time scale and unsupervised nature of UTL may allow rapid advances in answering these questions, systematically characterizing the spatiotemporal sensory statistics that drive it, and understanding if and how it extends to other types of image tolerance (e.g., changes in object scale, pose) (*27*, *28*).

IT neurons "learn" to give similar responses to different visual shapes ("paired associates") when reward is used to explicitly teach monkeys to associate those shapes over long time scales [1 to 5 s between images; see, e.g., (*29*, *30*)], but sometimes without explicit instruction (*31*, *32*). A top-down explanation of the neuronal selectivity changes in our study is unlikely because animals performed tasks that were unrelated to the object images when the selectivity was probed, and the selectivity changes were present in the earliest part of the IT responses (~100 ms; fig S4). But UTL could be an instance of the same plasticity mechanisms that underlie "paired associate" learning; here, the "associations" are between object images at different retinal positions (which, in the real world, are typically images of the same object). However, UTL may be qualitatively different because (i) the learning is retinal position-specific; (ii) it operates over the much shorter time scales of natural visual exploration (~200 ms); and (iii) it is unsupervised in that, besides the visual world, no external "teacher" was used to direct the learning (e.g., no association-contingent reward was used, but we do not rule out the role of internal "teachers" such as efferent eye-movement signals). These distinctions are important because we naturally receive orders-of-magnitude more such experience (e.g., ~10^8 unsupervised temporal-contiguity saccadic "experiences" per year of life).

Our results show that targeted alteration of natural, unsupervised visual experience changes the position tolerance of IT neurons as predicted by the hypothesis that the brain uses a temporal contiguity learning strategy to build that tolerance in the first place. Several computational models show how such strategies can build tolerance (*6*–*11*), and such models can be implemented by means of Hebbian-like learning rules (*8*, *33*) that are consistent with spike-timing–dependent plasticity (*34*). One can imagine IT neurons using almost temporally coincident activity to learn which sets of its afferents correspond to features of the same object at different positions. The time course and task independence of UTL are consistent with synaptic plasticity (*35*, *36*), but our data do not constrain the locus of plasticity, and changes at multiple levels of the ventral visual stream are likely (*37*, *38*).

We do not yet know if UTL reflects mechanisms than are necessary for building tolerant representations. But these same experience manipulations change the position tolerance of human object perception—producing a tendency to, for example, perceive one object to be the

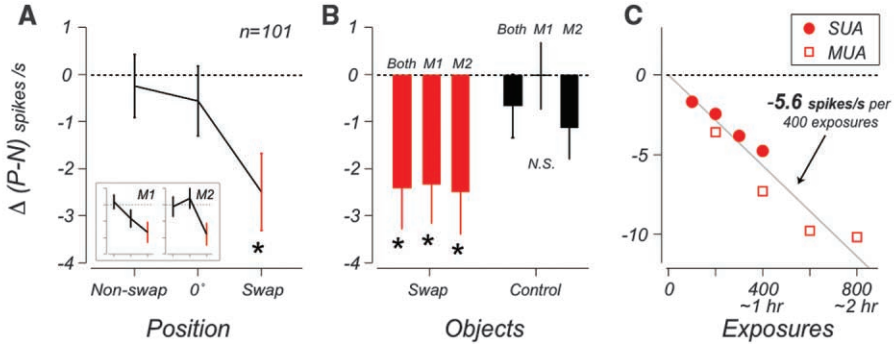

Fig. 3. Position specificity, object specificity, and time course. (**A**) Mean object selectivity change, Δ(P − N), at the swap, non-swap, and central (0°) retinal position. Δ(P − N) was computed as in Fig. 2C from each neuron's first and last available test phase (mean ~200 swap exposures). The insets show the same analysis performed separately for each monkey. (**B**) Mean object selectivity change for the (exposed) swap objects and (nonexposed) control objects at the swap position. Error bars (A and B) are SEMs. The swap object selectivity change at the swap position is statistically significant (*) in the pooled data as well as in individual animals ($P < 0.05$, one-tailed t test against 0). (**C**) Mean object selectivity change as a function of the number of swap exposures for all single-unit (n = 101) and multi-unit sites (n = 10). Each data point shows the average across all the neurons and sites held for a particular amount of time. Gray line is the best linear fit with a zero intercept; slope is mean effect size: −5.6 spikes/s per 400 exposures. The slope at the non-swap position based on the same analysis was 0.6 spikes/s (not shown).

Downloaded from www.sciencemag.org on October 16, 2008

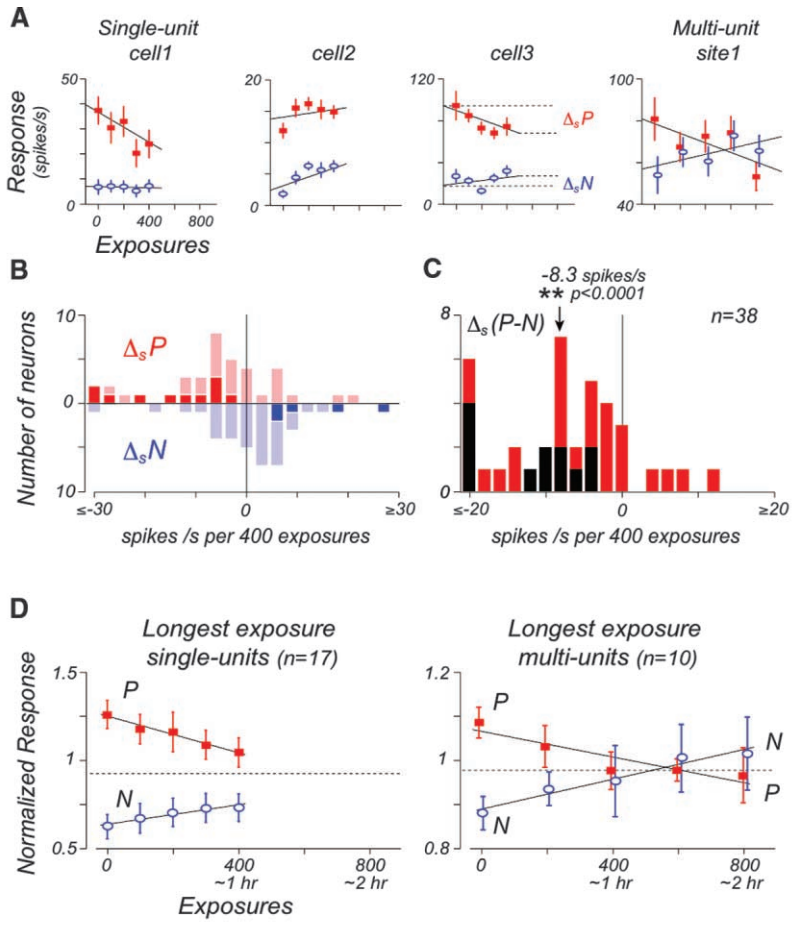

Fig. 4. Responses to objects P and N. (**A**) Response data to object P and N at the swap position for three example neurons and one multi-unit site as a function of exposure time. The solid line is standard linear regression. The slope of each line (Δ_S) provides a measure of the response change to object P and N for each neuron. Some neurons showed a response decrease to P, some showed a response enhancement to N, and others showed both (see examples). (**B**) Histograms of the slopes obtained for the object-selective neurons/sites tested for at least 300 exposures. The dark-colored bars indicate neurons with significant change by permutation test ($P < 0.05$) (*16*). (**C**) Histograms of the slopes from linear regression fits to object selectivity (P – N) as a function of exposure time; units are the same as in (B). Arrow indicates the mean of the distribution [the mean Δ_S(P – N) at the non-swap position was –1.7 spikes/s, $P = 0.38$]. The black bars indicate instances (32%; 12 of 38 neurons and sites) that showed a significant change in object selectivity by permutation test ($P < 0.05$). Results were very similar when we discarded neurons and sites with greater initial selectivity at the swap position (fig. S8). (**D**) Data from all the neurons and sites that were tested for the longest exposure time. The plot shows the mean normalized response to object P and N as a function of exposure time (compare to Fig. 1C; see fig. S3 for data at the non-swap position and for control objects). Error bars (A and D) are SEMs.

same identity as another object across a swap position (*12*). Moreover, given that the animals had a lifetime of visual experience to potentially build their IT position tolerance, the strength of UTL is substantial (~5 spikes/s change per hour)—just 1 hour of UTL is comparable to attentional effect sizes (*39*) and is more than double that observed in previous IT learning studies over much longer training intervals (*40*–*42*). We do not yet know how far we can extend this learning, but just 2 hours of (highly targeted) unsupervised experience begins to reverse the object preferences of IT neurons (Fig. 4D). This discovery reemphasizes the importance of plasticity in vision (*4*, *32*, *35*, *37*, *40*, *41*, *43*, *44*) by showing that it extends to a bedrock property of the adult ventral visual stream—position-tolerant object selectivity (*45*–*47*), and studies along the postnatal developmental time line are now needed.

References and Notes

1. S. Thorpe, D. Fize, C. Marlot, *Nature* **381**, 520 (1996).
2. M. C. Potter, *J. Exp. Psychol. (Hum. Learn.)* **2**, 509 (1976).
3. C. P. Hung, G. Kreiman, T. Poggio, J. J. DiCarlo, *Science* **310**, 863 (2005).
4. N. K. Logothetis, D. L. Sheinberg, *Annu. Rev. Neurosci.* **19**, 577 (1996).
5. R. Q. Quiroga, L. Reddy, G. Kreiman, C. Koch, I. Fried, *Nature* **435**, 1102 (2005).
6. L. Wiskott, T. J. Sejnowski, *Neural Comput.* **14**, 715 (2002).
7. P. Foldiak, *Neural Comput.* **3**, 194 (1991).
8. G. Wallis, E. T. Rolls, *Prog. Neurobiol.* **51**, 167 (1997).
9. R. Wyss, P. Konig, P. F. Verschure, *PLoS Biol.* **4**, e120 (2006).
10. T. Masquelier, S. J. Thorpe, *PLoS Comp. Biol.* **3**, e31 (2007).
11. T. Masquelier, T. Serre, S. J. Thorpe, T. Poggio, *CBCL Tech. Report #269,* Massachusetts Institute of Technology (2007).
12. D. D. Cox, P. Meier, N. Oertelt, J. J. DiCarlo, *Nat. Neurosci.* **8**, 1145 (2005).
13. G. Wallis, H. H. Bulthoff, *Proc. Natl. Acad. Sci. U.S.A.* **98**, 4800 (2001).
14. M. Ito, H. Tamura, I. Fujita, K. Tanaka, *J. Neurophysiol.* **73**, 218 (1995).
15. H. Op de Beeck, R. Vogels, *J. Comp. Neurol.* **426**, 505 (2000).
16. Materials and methods are available as supporting material on *Science* Online.
17. J. J. DiCarlo, J. H. R. Maunsell, *Nat. Neurosci.* **3**, 814 (2000).
18. J. Ross, M. C. Morrone, M. E. Goldberg, D. C. Burr, *Trends Neurosci.* **24**, 113 (2001).
19. D. J. Tolhurst, J. A. Movshon, A. F. Dean, *Vision Res.* **23**, 775 (1983).
20. M. N. Shadlen, W. T. Newsome, *J. Neurosci.* **18**, 3870 (1998).
21. K. Tanaka, *Cereb. Cortex* **13**, 90 (2003).
22. G. Kreiman *et al.*, *Neuron* **49**, 433 (2006).
23. T. Moore, M. Fallah, *Proc. Natl. Acad. Sci. U.S.A.* **98**, 1273 (2001).
24. E. Kowler, E. Anderson, B. Dosher, E. Blaser, *Vision Res.* **35**, 1897 (1995).
25. J. L. Ringo, S. Sobotka, M. D. Diltz, C. M. Bunce, *J. Neurophysiol.* **71**, 1285 (1994).
26. T. Moore, A. S. Tolias, P. H. Schiller, *Proc. Natl. Acad. Sci. U.S.A.* **95**, 8981 (1998).
27. S. Edelman, S. Duvdevani-Bar, *Neural Comput.* **9**, 701 (1997).
28. G. Wallis, H. Bulthoff, *Trends Cogn. Sci.* **3**, 22 (1999).
29. K. Sakai, Y. Miyashita, *Nature* **354**, 152 (1991).
30. A. Messinger, L. R. Squire, S. M. Zola, T. D. Albright, *Proc. Natl. Acad. Sci. U.S.A.* **98**, 12239 (2001).
31. Y. Miyashita, *Nature* **335**, 817 (1988).
32. C. A. Erickson, R. Desimone, *J. Neurosci.* **19**, 10404 (1999).
33. W. Gerstner, R. Kempter, J. L. van Hemmen, H. Wagner, *Nature* **383**, 76 (1996).
34. H. Sprekeler, C. Michaelis, L. Wiskott, *PLoS Comp. Biol.* **3**, e112 (2007).
35. C. D. Meliza, Y. Dan, *Neuron* **49**, 183 (2006).
36. H. Markram, J. Lubke, M. Frotscher, B. Sakmann, *Science* **275**, 213 (1997).
37. T. Yang, J. H. Maunsell, *J. Neurosci.* **24**, 1617 (2004).
38. Z. Kourtzi, J. J. DiCarlo, *Curr. Opin. Neurobiol.* **16**, 152 (2006).
39. J. H. R. Maunsell, E. P. Cook, *Philos. Trans. R. Soc. Lond. B Biol. Sci.* **357**, 1063 (2002).
40. C. I. Baker, M. Behrmann, C. R. Olson, *Nat. Neurosci.* **5**, 1210 (2002).
41. E. Kobatake, G. Wang, K. Tanaka, *J. Neurophysiol.* **80**, 324 (1998).
42. N. Sigala, N. K. Logothetis, *Nature* **415**, 318 (2002).
43. E. T. Rolls, G. C. Baylis, M. E. Hasselmo, V. Nalwa, *Exp. Brain Res.* **76**, 153 (1989).
44. A. Seitz, T. Watanabe, *Trends Cogn. Sci.* **9**, 329 (2005).
45. M. Dill, M. Fahle, *Percept. Psychophys.* **60**, 65 (1998).
46. M. Dill, S. Edelman, *Perception* **30**, 707 (2001).
47. T. A. Nazir, J. K. O'Regan, *Spat. Vis.* **5**, 81 (1990).

48. We thank D. Cox, R. Desimone, N. Kanwisher, J. Maunsell, and N. Rust for helpful comments

Downloaded from www.sciencemag.org on October 16, 2008

and discussion, and J. Deutsch, B. Kennedy, M. Maloof, and R. Marini for technical support. This work was supported by the NIH (grant R01-EY014970) and The McKnight Endowment Fund for Neuroscience.

Supporting Online Material
www.sciencemag.org/cgi/content/full/321/5895/1502/DC1
Materials and Methods
SOM Text
Figs. S1 to 12
Tables S1 and S2
References and Notes

5 May 2008; accepted 15 August 2008
10.1126/science.1160028

Conformational Switch of Syntaxin-1 Controls Synaptic Vesicle Fusion

Stefan H. Gerber,[1]*† Jong-Cheol Rah,[2,3]*‡ Sang-Won Min,[1]*§ Xinran Liu,[1,4] Heidi de Wit,[5] Irina Dulubova,[6] Alexander C. Meyer,[3] Josep Rizo,[6,7] Marife Arancillo,[2] Robert E. Hammer,[6,7] Matthijs Verhage,[5] Christian Rosenmund,[2,3]# Thomas C. Südhof[1,4,8]¶#

During synaptic vesicle fusion, the soluble *N*-ethylmaleimide-sensitive factor–attachment protein receptor (SNARE) protein syntaxin-1 exhibits two conformations that both bind to Munc18-1: a "closed" conformation outside the SNARE complex and an "open" conformation in the SNARE complex. Although SNARE complexes containing open syntaxin-1 and Munc18-1 are essential for exocytosis, the function of closed syntaxin-1 is unknown. We generated knockin/knockout mice that expressed only open syntaxin-1B. Syntaxin-1B^{Open} mice were viable but succumbed to generalized seizures at 2 to 3 months of age. Binding of Munc18-1 to syntaxin-1 was impaired in syntaxin-1B^{Open} synapses, and the size of the readily releasable vesicle pool was decreased; however, the rate of synaptic vesicle fusion was dramatically enhanced. Thus, the closed conformation of syntaxin-1 gates the initiation of the synaptic vesicle fusion reaction, which is then mediated by SNARE-complex/Munc18-1 assemblies.

Intracellular membrane fusion reactions are carried out by interactions between SNARE [soluble *N*-ethylmaleimide–sensitive factor (NSF)–attachment protein receptor) and SM (Sec1-Munc18–like) proteins (*1*, *2*). In Ca^{2+}-triggered exocytosis in neurons and neuroendocrine cells, fusion is catalyzed by the formation of SNARE complexes from syntaxin-1, synaptosome-associated protein of 25 kDa (SNAP-25), and synaptobrevin/vesicle-associated membrane protein and the binding of the SM protein Munc18-1 to these SNARE complexes (*1*–*3*). Syntaxin-1 consists of two similar isoforms (syntaxin-1A and -1B) that are composed of an N-terminal α-helical domain (the H_{abc} domain) and a C-terminal SNARE motif and transmembrane region. Outside of the SNARE complex, syntaxin-1 assumes a "closed" conformation, in which the H_{abc} domain folds back onto the C-terminal SNARE motif (*4*, *5*). In the SNARE complex, by contrast, syntaxin-1 is "opened" (*6*). Munc18-1 interacts with syntaxin-1 alone in the closed conformation to form heterodimers (*3*, *4*) and additionally binds to SNARE complexes containing syntaxin-1 in the open conformation to form Munc18-1– SNARE complex assemblies (*7*, *8*), which are essential for exocytosis (*3*). The function of the closed conformation of syntaxin-1 and its binding to Munc18-1 remain unknown.

We used gene targeting to create mice that lack syntaxin-1A (syntaxin-1A^{KO}) and contain the LE mutation in syntaxin-1B, which renders it predominantly open (syntaxin-1B^{Open}) (fig. S1) (*9*). Studying littermate offspring from crosses of double-heterozygous syntaxin-1A^{KO} and -1B^{Open} mice, we found that homozygous syntaxin-1A^{KO} mice exhibited no decrease in survival (Fig. 1A) or other obvious phenotypes (figs. S2 and S3). The expendability of syntaxin-1A was unexpected in view of its high concentrations and proposed central functions (*10*–*14*) and indicated that syntaxin-1A may be functionally redundant with syntaxin-1B.

Homozygous mutant syntaxin-1B^{Open} mice were also viable but severely ataxic and developed lethal epileptic seizures after 2 weeks of age (Fig. 1A and fig. S3). The seizure phenotype of syntaxin-1B^{Open} mutant mice was recessive and independent of the syntaxin-1A^{KO}. Thus, syntaxin-1B was selectively essential, probably because it is more widely expressed than syntaxin-1A (*15*). In *Caenorhabditis elegans*, transgenic syntaxin-1^{Open} rescues unc-13 mutant worms from paralysis (*16*); however, crossing syntaxin-1B^{Open} mice with Munc13-1 knockout mice did not prevent Munc13-1 knockout–induced death (fig. S4).

The syntaxin-1A^{KO} mutation abolished syntaxin-1A expression (Fig. 1B), whereas the syntaxin-1B^{Open} mutation decreased syntaxin-1B levels (Fig. 1C). Both mutations produced a modest decrease in Munc18-1 levels but no major changes in other proteins (table S1). The syntaxin-1^{Open} mutation decreases formation of the Munc18-1–syntaxin-1 complex but not formation of SNARE complexes or Munc18-1–SNARE complex assemblies (fig. S5) (*3*, *8*). Consistent with this conclusion, less Munc18-1 was coimmunoprecipitated with syntaxin-1 in syntaxin-1B^{Open} mice, whereas other SNARE proteins coimmunoprecipitated normally (Munc18-1–SNARE complex assemblies are not stable during immunoprecipitations, and thus cannot be evaluated) (Fig. 1D and fig. S6).

Electron microscopy of cultured cortical neurons from littermate syntaxin-1B^{Open} and -1B^{WT} mice lacking syntaxin-1A revealed increased vesicle docking in syntaxin-1B^{Open} synapses (~25% increase) (Fig. 2, A to D). The size of the postsynaptic density also was increased (~20%) (Fig. 2E), whereas the density of docked vesicles per active zone length was unchanged (Fig. 2F). No other structural parameter measured differed between syntaxin-1B^{Open} and -1B^{WT} synapses; in particular, the number and intraterminal distribution of vesicles were unaltered (fig. S7). In chromaffin cells, however, the syntaxin-1B^{Open} mutation caused a large decrease in chromaffin vesicle docking, similar to that of the Munc18-1 knockout. Again, neither mutation altered the total number of chromaffin vesicles (Fig. 2, K and L). Synaptobrevin-2 knockout mice, analyzed in parallel as a negative control, did not change chromaffin vesicle docking but did increase the total number of chromaffin vesicles (Fig. 2L). Consistent with earlier findings (*17*–*20*), these results indicate that the Munc18-1–syntaxin-1 complex, but not the SNARE complex, functions in chromaffin vesicle docking. This function may not be apparent in vertebrate synapses because active zone proteins that are absent from chromaffin cells probably dock synaptic vesicles independent of their attachment to the Munc18-1–syntaxin-1 complex.

Measurements of spontaneous miniature excitatory postsynaptic currents (mEPSCs), excitatory postsynaptic currents (EPSCs) evoked by

[1]Department of Neuroscience, University of Texas Southwestern Medical Center, Dallas, TX 75390–9111, USA. [2]Department of Molecular and Human Genetics and Department of Neuroscience, Baylor College of Medicine, Houston, TX 77030, USA. [3]Department of Membrane Biophysics, Max-Planck-Institute for Biophysical Chemistry, 37077 Göttingen, Germany. [4]Department of Molecular Genetics, University of Texas Southwestern Medical Center, Dallas, TX 75390–9111, USA. [5]Department of Functional Genomics, Vrije Universiteit, 1081 Amsterdam, Netherlands. [6]Department of Biochemistry, University of Texas Southwestern Medical Center, Dallas, TX 75390–9111, USA. [7]Department of Pharmacology, University of Texas Southwestern Medical Center, Dallas, TX 75390–9111, USA. [8]Howard Hughes Medical Institute, University of Texas Southwestern Medical Center, Dallas, TX 75390–9111, USA.

*These authors contributed equally to this work.
†Present address: Abteilung Innere Medizin III, Universität Heidelberg, 69120 Heidelberg, Germany.
‡Present address: Developmental Synaptic Plasticity Section, National Institute of Neurological Disorders and Stroke, Bethesda, MD 20892, USA.
§Present address: University of California, San Francisco, Mission Bay Campus, San Francisco, CA 94158, USA.
¶Present address: Department of Molecular and Cellular Physiology and Neuroscience Institute, Stanford University, Palo Alto, CA 94304–5543, USA.
#To whom correspondence should be addressed. E-mail: rosenmun@bcm.tmc.edu (C.R.); tcs1@stanford.edu (T.C.S.)

Downloaded from www.sciencemag.org on October 16, 2008